

Effects of large-scale non-axisymmetric perturbations in the mean-field solar dynamo.

V.V. Pipin¹⁻⁴ and A.G. Kosovichev^{3,4,5}

¹Institute of Solar-Terrestrial Physics, Russian Academy of Sciences,

² Institute of Geophysics and Planetary Physics, UCLA, Los Angeles, CA 90065, USA

³W.W. Hansen Experimental Physics Laboratory, Stanford University, Stanford, CA 94305,
USA

⁴NASA Ames Research Center, Moffett Field, CA 94035, USA

⁵New Jersey Institute of Technology, Big Bear, CA 92314, USA

Received _____; accepted _____

Abstract

We explore a response of a non-linear non-axisymmetric mean-field solar dynamo model to shallow non-axisymmetric perturbations. After a relaxation period the amplitude of the non-axisymmetric field depends on the initial condition, helicity conservation, and the depth of perturbation. It is found that a perturbation which is anchored at the $0.9R_{\odot}$ has a profound effect on the dynamo process, producing a transient magnetic cycle of the axisymmetric magnetic field, if it is initiated at the growing phase of the cycle. The non-symmetric with respect to the equator perturbation results in a hemispheric asymmetry of the magnetic activity. The evolution of the axisymmetric and non-axisymmetric field depends on the turbulent magnetic Reynolds number R_m . In the range of $R_m = 10^{4-6}$ the evolution returns to the normal course in the next cycle, in which the non-axisymmetric field is generated due to a non-linear α -effect and magnetic buoyancy. In the stationary state the large-scale magnetic field demonstrates a phenomenon of “active longitudes” with cyclic 180° “flip-flop” changes of the large-scale magnetic field orientation. The flip-flop effect is known from observations of solar and stellar magnetic cycles. However this effect disappears in the model which includes the meridional circulation pattern determined by helioseismology. The rotation rate of the non-axisymmetric field components varies during the relaxation period, and carries important information about the dynamo process.

1. Introduction

Dynamo theories commonly assume that the magnetic activity of the Sun is approximately axisymmetric on large spatial (size of the Sun) and temporal (the period of solar cycle) scales. These models provide quantitative self-consistent description of the 22-year solar magnetic cycles, and allow us to investigate the basic mechanisms of the solar dynamo. However, deviations from the axisymmetry are rather strong at any particular moment of observations. Intermittent patterns of magnetic fields on the solar surface are formed because the magnetic field emerges on the surface like separated magnetic patches, e.g, in the form of sunspot groups. Such phenomena make a significant contribution to the large-scale non-axisymmetric magnetic field of the Sun. Thus, studying properties of the non-axisymmetric field can shed light on the origin of solar active regions, their clustering, “active longitudes”, sector structure of the heliosphere, etc.. Knowledge of the angular velocity distribution and the meridional circulation inside the Sun provided by helioseismology is essential for the solar dynamo models. Observations have shown that large-scale magnetic fields in the Northern and Southern hemispheres rotate with different speeds (Antonucci et al. 1990). The magnitude and rotation rate of the large-scale non-axisymmetric magnetic field can bring new information about the dynamo process inside the convection zone. This question has not been addressed in mean-field models of the large-scale solar dynamo. Theoretically, it was argued that the solar dynamo is likely to operate in the so-called $\alpha\Omega$ or $\alpha^2\Omega$ regimes (Raedler 1986; Raedler et al. 1990). In these regimes the non-axisymmetric dynamo modes are likely to be linearly-stable because of a profound effect of the differential rotation on the large-scale magnetic field. The previous non-linear solar dynamo models showed that a weak non-axisymmetric magnetic field can co-exists with the global axisymmetric field (Raedler et al. 1990; Moss 1999; Elstner & Korhonen 2005). The nonlinear models predict that the energy of the non-axisymmetric modes is only about 10^{-4} of the energy of the axisymmetric component (Berdyugina et al.

2006). Observations at the Wilcox Solar Observatory (Duvall et al. 1979; Hoeksema 1995) found that the strength of the $m=1$ non-axisymmetric mode can be about 1-2 G during epoch of the solar maxima. The axisymmetric dipole has the same magnitude during the solar minima. It is likely that the origin of this non-axisymmetric field is related to decay of solar active regions. However it is unclear how the evolution of such non-axisymmetric field may impact the solar dynamo process. The effect of non-axisymmetric field on the global dynamo has not been studied before.

In this paper we explore a non-linear response of the dynamo model to a shallow non-axisymmetric perturbations with the magnetic field strength of 1G. We consider a fairly complete theoretical description of the mean turbulent electro-motive force taking into account the known properties of the solar convection zone and including the anisotropic turbulent effects due to the global rotation. The model includes a nonlinear magnetic buoyancy effect, and two types of nonlinearity in the α -effect, described as “algebraic” and “dynamical” quenching (Tworkowski et al. 1998). The algebraic quenching is due to the back-reaction of the dynamo-generated magnetic field on helical turbulence. The dynamical quenching results from a magnetic helicity conservation condition (Kleeorin & Ruzmaikin 1982). We will show that given nonlinear non-axisymmetrical effects are sufficiently strong to reproduce the “flip-flop” phenomenon and explain the rotation rate of active longitudes on the Sun (Tuominen et al. 2002; Berdyugina et al. 2006; Gyenge et al. 2012).

2. Basic equations

Evolution of the large-scale magnetic field in perfectly conductive media is described by the mean-field induction equation (Krause & Rädler 1980; Moffatt 1978; Parker 1979):

$$\partial_t \langle \mathbf{B} \rangle = \nabla \times (\mathcal{E} + \langle \mathbf{U} \rangle \times \langle \mathbf{B} \rangle) \quad (1)$$

where $\boldsymbol{\mathcal{E}} = \langle \mathbf{u} \times \mathbf{b} \rangle$ is the mean electromotive force; \mathbf{u} and \mathbf{b} are the turbulent fluctuating velocity and magnetic field respectively; and $\langle \mathbf{U} \rangle$ and $\langle \mathbf{B} \rangle$ are the mean velocity and magnetic field. Our solution of the dynamo equation will follow the outline given earlier by Moss et al. (1991) and Moss (1999). For convenience we decompose the magnetic field into the axisymmetric, (hereafter $\bar{\mathbf{B}}$ -field), and non-axisymmetric parts, (hereafter $\tilde{\mathbf{B}}$ -field): $\langle \mathbf{B} \rangle = \bar{\mathbf{B}} + \tilde{\mathbf{B}}$. We assume that the mean flow is axisymmetric $\langle \mathbf{U} \rangle \equiv \bar{\mathbf{U}}$. Let $\hat{\phi} = \mathbf{e}_\phi$ and $\hat{\mathbf{r}} = r\mathbf{e}_r$ be vectors in the azimuthal and radial directions respectively, then we represent the mean magnetic field vectors as follows:

$$\langle \mathbf{B} \rangle = \bar{\mathbf{B}} + \tilde{\mathbf{B}} \quad (2)$$

$$\bar{\mathbf{B}} = \hat{\phi}B + \nabla \times (A\hat{\phi}) \quad (3)$$

$$\tilde{\mathbf{B}} = \nabla \times (\hat{\mathbf{r}}T) + \nabla \times \nabla \times (\hat{\mathbf{r}}S), \quad (4)$$

where A , B , T and S are scalar functions representing the axisymmetric and non-axisymmetric parts respectively. Assuming that A and B do not depend on longitude, Eqs(3, 4) ensure that the field $\langle \mathbf{B} \rangle$ is divergence-free. Taking the scalar product of Eq(1) with vector $\hat{\phi}$ we get equations for the axisymmetric magnetic field components,

$$\partial_t B = \hat{\phi} \cdot \nabla \times (\boldsymbol{\mathcal{E}} + \bar{\mathbf{U}} \times \bar{\mathbf{B}}), \quad (5)$$

$$\partial_t A = \hat{\phi} \cdot (\boldsymbol{\mathcal{E}} + \bar{\mathbf{U}} \times \bar{\mathbf{B}}), \quad (6)$$

To get equation for T we take curl of the Eq(1), and then calculate scalar product with vector $\hat{\mathbf{r}}$. Similarly, equation for S is obtained by taking twice curl of Eq(1) and then the scalar product with vector $\hat{\mathbf{r}}$. The procedure is described in detail by Krause & Rädler (1980). Equations for the non-axisymmetric field are

$$\partial_t \Delta_\Omega T = \Delta_\Omega V^{(U)} + \Delta_\Omega V^{(\mathcal{E})}, \quad (7)$$

$$\partial_t \Delta_\Omega S = \Delta_\Omega U^{(U)} + \Delta_\Omega U^{(\mathcal{E})}, \quad (8)$$

where $\Delta_\Omega = \frac{\partial}{\partial \mu} \sin^2 \theta \frac{\partial}{\partial \mu} + \frac{1}{\sin^2 \theta} \frac{\partial^2}{\partial \phi^2}$, $\mu = \cos \theta$ and θ is a polar angle, and

$$\Delta_\Omega V^{(U)} = -\hat{\mathbf{r}} \cdot \nabla \times \nabla \times (\bar{\mathbf{U}} \times \tilde{\mathbf{B}}), \quad (9)$$

$$\Delta_\Omega V^{(\mathcal{E})} = -\hat{\mathbf{r}} \cdot \nabla \times \nabla \times \mathcal{E}, \quad (10)$$

$$\Delta_\Omega U^{(U)} = -\hat{\mathbf{r}} \cdot \nabla \times (\bar{\mathbf{U}} \times \tilde{\mathbf{B}}), \quad (11)$$

$$\Delta_\Omega U^{(\mathcal{E})} = -\hat{\mathbf{r}} \cdot \nabla \times \mathcal{E}. \quad (12)$$

The scalar functions with superscript (U) contain contributions from the large-scale axisymmetric flows like the differential rotation or meridional circulation. The integration domain includes the solar convection zone from 0.71 to $0.99R_\odot$. The distribution of the mean flows is given by helioseismology (Howe et al. 2011 and Zhao et al. 2013). Profiles of the angular velocity and meridional circulation are illustrated in Figure 1.

We use formulation for the mean electromotive force obtained by Pipin(2008). The calculations of the mean electromotive force are done using the mean-field magnetohydrodynamics framework and the so-called “minimal tau-approximation” (see, e.g., Blackman & Field 2002; Rädler et al. 2003; Brandenburg & Subramanian 2005). The tau-approximation suggests that the second-order correlations do not vary significantly on timescale τ_c which corresponds to a typical turnover time of the convective flows. The theoretical calculations are performed for anelastic turbulent flows. They take into account the effects of density stratification, spatial inhomogeneity of the intensity of turbulent flows, and inhomogeneity of the large-scale magnetic fields. The effects of large-scale inhomogeneity of the turbulent flows and magnetic fields are computed in the first order of the Taylor expansion in terms of ratio ℓ/L , where ℓ is a typical spatial scale of the turbulence, and L is a spatial scale of the mean quantities. The mean electromotive force, \mathcal{E} , is expressed as follows (Pipin, 2008):

$$\mathcal{E}_i = (\alpha_{ij} + \gamma_{ij}) \langle B \rangle_j - \eta_{ijk} \nabla_j \langle B \rangle_k. \quad (13)$$

where symmetric tensor α_{ij} models the generation of magnetic field by the α - effect; antisymmetric tensor γ_{ij} controls the mean drift of the large-scale magnetic fields in turbulent medium; tensor η_{ijk} governs the turbulent diffusion. We take into account the effect of rotation and magnetic field on the mean-electromotive force (see Appendix for details). To determine unique solution of Eqs.(5-8) we apply the following gauge (see, e.g., Krause & Rädler 1980; Bigazzi & Ruzmaikin 2004):

$$\int_0^{2\pi} \int_{-1}^1 S d\mu d\phi = 0, \quad \int_0^{2\pi} \int_{-1}^1 T d\mu d\phi = 0. \quad (14)$$

The same gauge is used in Eqs(9-12).

2.1. Nonlinear interaction of the axisymmetric and non-axisymmetric modes

Interaction between the axisymmetric and non-axisymmetric modes in the mean-field dynamo models can be due to nonlinear dynamo effects, for example, the α -effect, (Krause & Rädler 1980; Moss 1999). In our model the α effect takes into account the kinetic and magnetic helicities in the following form:

$$\alpha_{ij} = C_\alpha \sin^2 \theta \psi_\alpha(\beta) \alpha_{ij}^{(H)} \eta_T + \alpha_{ij}^{(M)} \frac{\langle \chi \rangle \tau_c}{4\pi \bar{\rho} \ell^2} \quad (15)$$

where C_α is a free parameter which controls the strength of the α - effect due to turbulent kinetic helicity; $\alpha_{ij}^{(H)}$ and $\alpha_{ij}^{(M)}$ express the kinetic and magnetic helicity parts of the α -effect, respectively; η_T is the magnetic diffusion coefficient, and $\langle \chi \rangle = \langle \mathbf{a} \cdot \mathbf{b} \rangle$ (\mathbf{a} and \mathbf{b} are the fluctuating parts of magnetic field vector-potential and magnetic field vector). Both the $\alpha_{ij}^{(H)}$ and $\alpha_{ij}^{(M)}$ depend on the Coriolis number $\Omega^* = 4\pi \frac{\tau_c}{P_{rot}}$, where P_{rot} is the rotational period, τ_c is the convective turnover time, and ℓ is a typical length of the convective flows (the mixing length). A theoretical justification for the latitudinal factor, $\sin^2 \theta$, in Eq(15) was given by Kleorin & Rogachevskii (2003). Function $\psi_\alpha(\beta)$, controls the so-called “algebraic” quenching of the α - effect where $\beta = |\langle \mathbf{B} \rangle| / \sqrt{4\pi \bar{\rho} u'^2}$, u' is the RMS of the

convective velocity. For the case of the strong magnetic field, $\beta \gg 1$, $\psi_\alpha \sim \beta^{-2}$. The interaction between the axisymmetric and non-axisymmetric dynamo modes via $\psi_\alpha(\beta)$ is because both modes contribute to parameter β . Also, for the case $\beta > 1$, the latitudinal profile of the α effect changes. This can affect the dynamo conditions for excitation of the non-axisymmetric modes. Raedler et al. (1990) and Moss (1999) discussed the evolution of non-axisymmetric magnetic field in a simple dynamo model with such “algebraic” quenching.

The dynamical quenching is caused by the magnetic helicity conservation (see, Kleeorin & Ruzmaikin 1982). This effect was discovered by Frisch et al. (1975) and Pouquet et al. (1975). Contribution of the magnetic helicity to the α -effect is expressed by the second term in Eq.(15). The magnetic helicity density of turbulent field, $\langle \chi \rangle = \langle \mathbf{a} \cdot \mathbf{b} \rangle$, is governed by the conservation law (Hubbard & Brandenburg 2012; Pipin et al. 2013):

$$\frac{\partial \langle \chi \rangle^{(tot)}}{\partial t} = -\frac{\langle \chi \rangle}{R_m \tau_c} - 2\eta \langle \mathbf{B} \rangle \cdot \langle \mathbf{J} \rangle - \nabla \cdot \mathcal{F}^\chi, \quad (16)$$

where $\langle \chi \rangle^{(tot)} = \langle \chi \rangle + \langle \mathbf{A} \rangle \cdot \langle \mathbf{B} \rangle$ is the total magnetic helicity density of the mean and turbulent fields, $\mathcal{F}^\chi = -\eta_\chi \nabla \langle \chi \rangle$ is the diffusive flux of the turbulent magnetic helicity, and R_m is the magnetic Reynolds number. The coefficient of the turbulent helicity diffusivity, η_χ , is chosen ten times smaller than the isotropic part of the magnetic diffusivity (Mitra et al. 2010): $\eta_\chi = \frac{1}{10} \eta_T$. Similarly to the magnetic field, the mean magnetic helicity density can be formally decomposed into the axisymmetric and non-axisymmetric parts: $\langle \chi \rangle^{(tot)} = \bar{\chi}^{(tot)} + \tilde{\chi}^{(tot)}$. The same can be done for the magnetic helicity density of the turbulent field: $\langle \chi \rangle = \bar{\chi} + \tilde{\chi}$, where $\bar{\chi} = \overline{\mathbf{a} \cdot \mathbf{b}}$ and $\tilde{\chi} = \langle \mathbf{a} \cdot \tilde{\mathbf{b}} \rangle$. Then we have,

$$\bar{\chi}^{(tot)} = \bar{\chi} + \overline{\mathbf{A} \cdot \mathbf{B}} + \overline{\tilde{\mathbf{A}} \cdot \tilde{\mathbf{B}}}, \quad (17)$$

$$\tilde{\chi}^{(tot)} = \tilde{\chi} + \overline{\mathbf{A} \cdot \tilde{\mathbf{B}}} + \overline{\tilde{\mathbf{A}} \cdot \mathbf{B}} + \overline{\tilde{\mathbf{A}} \cdot \tilde{\mathbf{B}}}, \quad (18)$$

Evolution of the $\bar{\chi}$ and $\tilde{\chi}$ is governed by the corresponding parts of Eq(16). Thus, the model takes into account contributions of the axisymmetric and non-axisymmetric fields

in the whole magnetic helicity density balance, providing a non-linear coupling. We see that the α -effect is dynamically linked to the longitudinally averaged magnetic helicity of the non-axisymmetric $\tilde{\mathbf{B}}$ -field, which is the last term in Eq(17). Thus, the nonlinear α -effect is non-axisymmetric, and it results in coupling between the axisymmetric and non-axisymmetric modes. The coupling works in both directions. For instance, the azimuthal α -effect results in $\mathcal{E}_\phi = \alpha_{\phi\phi} \langle B_\phi \rangle$. If we denote the non-axisymmetric part of the $\alpha_{\phi\phi}$ by $\tilde{\alpha}_{\phi\phi}$ then the mean electromotive force is $\overline{\mathcal{E}}_\phi = \overline{\alpha}_{\phi\phi} \overline{B}_\phi + \overline{\tilde{\alpha}_{\phi\phi} \tilde{B}_\phi}$. This introduces a new source in Eq(6) which is usually ignored in the axisymmetric dynamo models.

Magnetic buoyancy is another nonlinear effect which is important in the large-scale dynamo. The part of the mean electro-motive force which is responsible for magnetic buoyancy is (Kichatinov & Pipin 1993):

$$\boldsymbol{\mathcal{E}}^{(\beta)} = V_\beta \hat{\mathbf{r}} \times \mathbf{B}, \quad (19)$$

where $V_\beta = C_\beta \frac{\alpha_{MLT} u'}{\gamma} \beta^2 K(\beta)$, u' is the RMS convection velocity, $K(\beta)$ is given in Appendix, γ is the adiabatic exponent, α_{MLT} is the mixing-length theory parameter, C_β is a free parameter to switch on/off this effect in the model. For the case $\beta \ll 1$, $K \sim 1$ and the upflow velocity, V_β , is proportional to the pressure of large-scale magnetic field. Similarly to the α -effect, the V_β is non-axisymmetric and contributes to the source terms in Eqs(5,6). Note that advection of the large-scale magnetic field by the magnetic buoyancy reduces concentration of the magnetic field near the bottom of the convection zone, and increases the field strength near the top.

2.2. Parameters of the convection zone and numerical procedure

The distribution of the turbulent parameters, such as the typical convective turn-over time, τ_c , the mixing length, ℓ , and the RMS convection velocity, u' , are taken from the

solar interior model of Stix (2002). We define the mixing-length: $\ell = \alpha_{\text{MLT}} |\Lambda^{(p)}|^{-1}$, where $\Lambda^{(p)} = \nabla \log \bar{p}$ is the inverse pressure scale, and the mixing-length parameter $\alpha_{\text{MLT}} = 2$. The profile of the turbulent diffusivity is taken in the form $\eta_T = C_\eta \frac{u'^2 \tau_c}{3 f_{ov}(r)}$, where $f_{ov}(r) = 1 + \exp[50(r_{ov} - r)]$, $r_{ov} = 0.725 R_\odot$ controls quenching of the turbulent effects near the bottom of the convection zone, which is $r_b = 0.715 R_\odot$. Free parameter C_η , ($0 < C_\eta < 1$) controls the efficiency of mixing of the large-scale magnetic field by turbulence. It is usually employed to tune the period of the dynamo cycle.

The numerical scheme employs the spherical harmonics decomposition for the non-axisymmetric part of the problem, i.e., the scalar functions T and S in Eqs(7,8) are represented in the form:

$$T(r, \mu, \phi, t) = \sum \hat{T}_{l,m}(r, t) \bar{P}_l^{|m|} \exp(im\phi), \quad (20)$$

$$S(r, \mu, \phi, t) = \sum \hat{S}_{l,m}(r, t) \bar{P}_l^{|m|} \exp(im\phi), \quad (21)$$

where \bar{P}_l^m is the normalized associated Legendre function of degree $l \geq 1$ and order $m \geq 1$. The simulations which we will discuss include 600 spherical harmonics ($l_{max} = 28$). Note that $\hat{S}_{l,-m} = \hat{S}_{l,m}^*$ and the same for \hat{T} . We employ the pseudo-spectral approach for integration along latitude. The second-order finite differences are used for discretization in the radial direction. The numerical integration is carried out in latitude from the pole to pole and in radius from $r_b = 0.715 R_\odot$ to $r_e = 0.99 R_\odot$. All the nonlinear terms are calculated in the real space. The transformation between the spectral spherical harmonic and the real 3D space was done using the Intel Fortran FFT library. We implement algorithms of Muciaccia et al. (1997) to speed-up the transform calculations. At the bottom of the convection zone we set up a perfectly conducting boundary condition for the axisymmetric magnetic field, and for the non-axisymmetric field we set the functions S and T to zero. At the top of the convection zone the poloidal field is smoothly matched to the external potential field. The boundary conditions for toroidal field allow field penetrate the surface

(Moss et al. (1991), Pipin & Kosovichev (2011)):

$$\delta \frac{\eta_T}{r_e} B + (1 - \delta) \mathcal{E}_\theta = 0, \quad (22)$$

$$\frac{\delta}{R} T - (1 - \delta) \frac{\partial T}{\partial r} = 0 \quad (23)$$

where parameter $\delta = 0.99$.

The particular choice of parameters was discussed in our previous papers (see, e.g, Pipin & Kosovichev 2014). The free parameters are $C_\alpha = 0.04$, $C_\delta = \frac{1}{3}C_\alpha$, $C_\eta = \frac{1}{15}$ and the anisotropy parameter $a = 3$ (see Eqs(A5-A1)). The α -effect parameter C_α is about 30% above the dynamo generation threshold. For the chosen values of C_η and a , the turbulent diffusion coefficient in the near-surface shear layer, at $r = 0.9R_\odot$ is about $10^9 \text{m}^2 \text{s}^{-1}$ which is in agreement with surface observations (see, Abramenko et al. 2011). The magnetic helicity conservation is determined by the magnetic Reynolds number R_m , for which we considered values: 10^4 - 10^6 . To investigate the influence of meridional circulation we consider two models (Table 1): M1 without meridional circulation and M2 with the double-cell meridional circulation with a characteristic velocity 10 m/s.

2.3. Initial conditions

In our first runs the weak initial field, which consisted of a superposition sum of polar and equatorial dipoles with the magnetic field strength of 0.01G, evolved to a state in which the axisymmetric dynamo regime dominates. In this regime, the typical strength of the axisymmetric toroidal field in the convection zone is about 1kG. However, the non-axisymmetric field is rather weak with the strength about 10^{-6} G. This means that in our model the non-axisymmetric magnetic field is linearly stable, unless the dynamo governing parameters are forced to be non-axisymmetric, e.g., like in the paper by Bigazzi

& Ruzmaikin (2004).

Exploring the nonlinear solutions we found that the evolution of the non-axisymmetric field depends on the initial conditions which includes the strength and geometry of both the axisymmetric $\bar{\mathbf{B}}$ -field and non-axisymmetric $\tilde{\mathbf{B}}$ -field. The evolution of the large-scale magnetic field depends on the presence of the meridional circulation, too.

In the following section we present results for the non-axisymmetric dynamo which was perturbed by a finite-amplitude non-axisymmetric $\tilde{\mathbf{B}}$ -field in the developed axisymmetric dynamo regime. Such non-axisymmetric perturbations can be developed either due to evolution of active regions or due to instabilities not described by the mean-field theory (e.g., Dikpati & Gilman 2001). For the seed field we consider a non-symmetric relative to the equator perturbation represented by a sum of the equatorial dipole ($l=1, m=\pm 1$) and quadrupole ($l=2, m=\pm 1$) components. In Eq(21) we define

$$S_{1,1} = \left(1 - \operatorname{erf} \left(\frac{(r_s - r_e)}{d} \right) \right) \frac{r_e}{r}, \quad (24)$$

$$S_{1,2} = \left(1 - \operatorname{erf} \left(\frac{(r_s - r_e)}{d} \right) \right) \left(\frac{r_e}{r} \right)^2, \quad (25)$$

where, $r_e = 0.99R_\odot$, $r_s = 0.9R_\odot$ is the bottom of the subsurface shear layer, $d = 0.02R_\odot$.

The other $S_{l,m}$ and $T_{l,m}$ are zero in the perturbation. The initial non-axisymmetric perturbation is concentrated in the near-surface shear layer. The depth of the non-axisymmetric perturbation can influence the evolution of the axisymmetric dynamo.

3. Results

Figure 2 illustrates the geometry of the axisymmetric and non-axisymmetric fields just before initialization of the non-axisymmetric perturbation. Figure 3 illustrates the evolution of the axisymmetric magnetic field before and after the perturbation for two

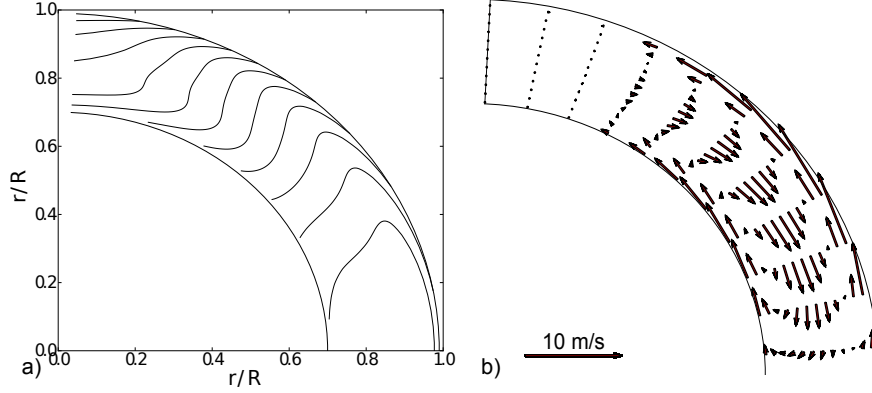


Fig. 1.— a) The isolines of constant angular velocity ranging from $0.6\Omega_0$ to $0.96\Omega_0$ ($\Omega_0 = 2.87 \times 10^{-6}\text{s}^{-1}$); b) illustration of the double-cell meridional circulation model, consistent with helioseismology results of Zhao et al (2013).

Table 1: Summary of the dynamo models and their parameters.

Components	M1	M2
α_{ij} -effect	Eqs.(15,16,A6,A7)	same
η_{ijk} -diffusivity	Eqs.(A1)	same
γ_{ij} -pumping	Eqs.(A17)	same
circulation	no	$\bar{U} = 10\text{m/s}$
free parameters	$C_\alpha = 0.04, C_\delta = C_\alpha/3,$ $C_\eta = 0.06, a=3, C_\beta = 1$ and $C_\beta = C_\eta, R_m = 10^{4-6},$ $\alpha_{MLT} = 2$	$C_\alpha = 0.05, C_\beta = 1$, others are same as in M1

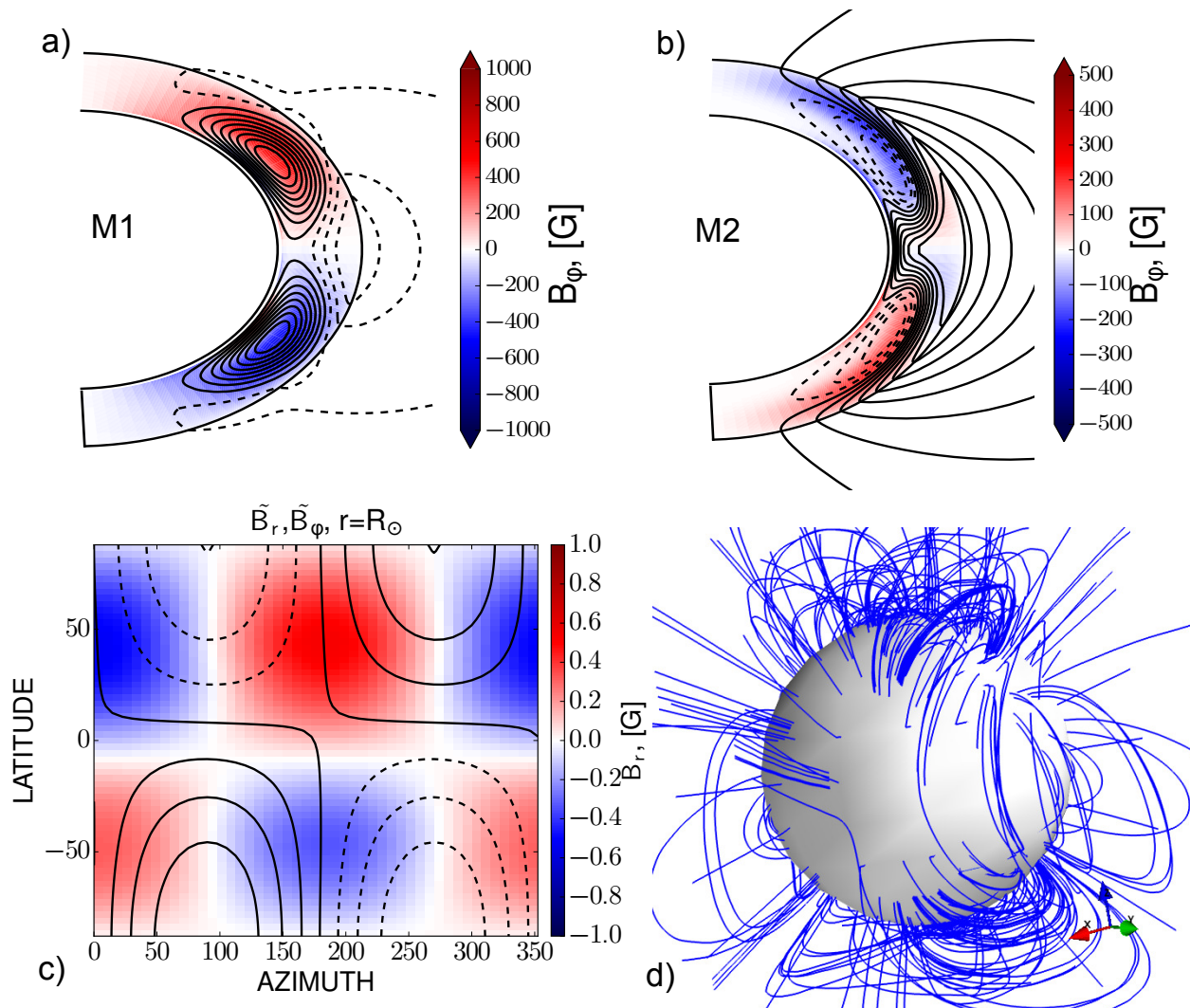


Fig. 2.— Axisymmetric and non-axisymmetric field structure at the moment of initialization of the non-axisymmetric perturbation: a) model M1, distribution of the axisymmetric toroidal magnetic field (background image) and poloidal field lines in the meridional cross-section; b) the same as a) for model M2; c) components of non-axisymmetric magnetic at the surface; d) illustration of the magnetic field lines of the perturbation.

models, with and without the meridional circulation. We show the time-latitude diagrams for the toroidal magnetic field in the subsurface shear layer and the radial magnetic field at the surface. In the model with the meridional circulation the toroidal magnetic field is shown for the middle of the convection zone (see Pipin & Kosovichev 2013). The radial evolution is shown for 30° latitude in the Northern hemisphere. We simulate the sunspot number W using the ansatz (Pipin et al. 2012):

$$W(t) = \langle B_{\max} \rangle_{SL} \exp\left(-\frac{B_0}{\langle B_{\max} \rangle_{SL}}\right), \quad (26)$$

where in the model M1 $\langle B_{\max} \rangle_{SL}$ is the maximum strength of the toroidal magnetic field averaged over radius in the subsurface layers in the range of $0.9 - 0.99R_\odot$, and in the model M2 it is the same for the middle of the convection zone; B_0 a characteristic strength of the toroidal magnetic field, $B_0 = 800\text{G}$.

The models show that the imposed non-axisymmetric perturbation produces a transient cycle in both models M1 and in M2. In the Northern hemisphere where the initiated perturbation is greater the simulated sunspot number cycle is stronger than in the Southern hemisphere. The perturbation affects the reversal of the polar magnetic fields. In the Northern hemisphere the polar field reversal occurs earlier than in the Southern hemisphere where we see multiple reversals. The models show a time shift of about 2 years for the polar reversals in the Northern and Southern hemispheres. We find that these phenomena depend on the depth of perturbation (parameters, r_s and d in Eq(24)). For instance, the polar field reversal happens earlier in the Southern hemisphere than in the Northern one if the imposed perturbation is shallower $r_s = 0.95R_\odot$. We also see that in model M1 the cycle returns quickly to the previously established axisymmetric state. In model M2 with the meridional circulation, the restoration process takes longer than in model M1. In that model for $R_m = 10^4$, the normal cycles are restored about 40 years after the perturbation. For higher R_m the relaxation time in both models goes is similar. Figure 4 illustrates the

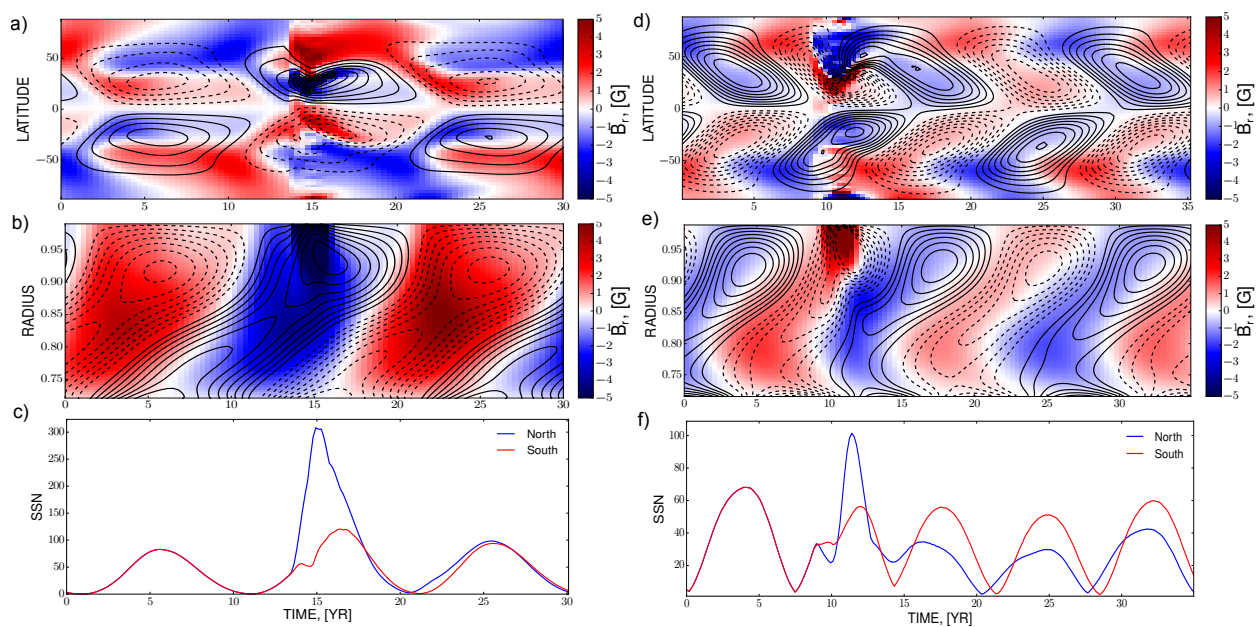


Fig. 3.— . a-c) Dynamo evolution in model M1 before and after the initialization of the non-axisymmetric perturbation at $t=13$ yr: a) time-latitude diagram, b) time-radius diagram at 30° latitude, c) the simulated sunspot number for the Northern and Southern hemispheres; d-f) show the same for model M2. Color images show the radial magnetic field component. The contour lines show the toroidal component.

results for model M1 for $R_m = 10^4$ and $R_m = 10^6$ and also for model M1 with a reduced magnetic buoyancy effect ($C_\beta = C_\eta$). The developed axisymmetric dynamo regime which is employed at the beginning of evolution series shown in Figure 4 is related to the the case $R_m = 10^4$ and $C_\beta = 1$. This explains why magnetic cycles in model M1 with $C_\beta = C_\eta$ and $R_m = 10^6$ do not relax to the original cycle amplitude. The model with a reduced magnetic buoyancy shows a smaller (by a factor 2) magnitude of $T_{1,1}$ mode after the relaxation. The mode $T_{1,1}$ shows a larger variations of amplitude in case of $R_m = 10^6$ than in the case of $R_m = 10^4$ after relaxation.

The restoration of the initial of the axisymmetric magnetic field evolution after the perturbation does not mean that the non-axisymmetric field completely dissipates. Figures 5(a,c) and 6(a,c) show that a low strength non-axisymmetric field is maintained in the model. We find that the strength of the toroidal field T-potentials is reduced from about 10G at the maximum to 0.01G after the relaxation. Even such a low strength non-axisymmetric magnetic field can produce some interesting phenomena which may be related to solar observations.

Figures 5(b,d) and 6(b,d) shows the evolution of longitude of a maximum of the large-scale toroidal field and the latitude-longitude position of the maxima of the large-scale toroidal magnetic field strength in the subsurface shear layer. Model M1 (without the meridional circulation) shows the periodic changes of the longitudes by 180° degrees during the magnetic cycle decay. The change of the longitude is accompanied by a change of the hemispheric position of the field maximum. Thus, the orientation of the global non-axisymmetric field is reversed every cycle during the minima of the toroidal magnetic field. This behavior may correspond to the “flip-flop” phenomenon of the active longitudes observed in stellar magnetic cycles (Berdyugina 2004).

Model M2 which includes the meridional circulation has no stable positions of the

non-axisymmetric magnetic field azimuth. Figures 5(a) and 6(a) clarify the reason for this. The effect disappears because the circulation mixes the magnetic field in the subsurface shear layer with the magnetic field of the deep interior with a period which approximately corresponds to the period of the magnetic cycle. We see that oscillations of the $S_{1,1}$ and $T_{1,1}$ harmonics have a $\pi/2$ phase shift. Thus, for a persistent appearance of the active longitude the phases of the $S_{1,1}$ and $T_{1,1}$ harmonics should be consistent. Model M2 shows a continuous drift of the longitude of the large-scale toroidal magnetic field strength in the course of the magnetic activity evolution.

Figure 7 shows snapshots of the axisymmetric and non-axisymmetric fields after a half-year evolution of the initial perturbation. We also show configuration of the external potential field which corresponds to the non-axisymmetric component of magnetic field. This period of time corresponds to a maximum of the toroidal magnetic field in the upper part of the convection zone, and the epoch of the polar field reversal. The non-axisymmetric part of the field is concentrated to the surface (as the initial field). The longitude-latitude diagram shows distributions of the large-scale non-axisymmetric magnetic field. It illustrates how the differential rotation stretches the initial magnetic field configuration (cf., Fig2a). Snapshots show the large-scale unipolar regions which extend from the equator to the poles. The increasing of the non-axisymmetric magnetic field in the polar regions results in twisted field lines going from the polar caps.

Figure 9 illustrates snapshots of the magnetic field configuration during the decaying phase of the magnetic cycle in model M1 after 5 years from the initialization. We see that the non-axisymmetric toroidal field distributed over the convection zone has maxima at the bottom of the convection zones and in the near equatorial region. The strength of the non-axisymmetric field is much smaller than of the axisymmetric field. Model M2 has long overlaps between the subsequent cycles. Snapshots for this model are shown in

Fig.9(bottom) for the growing phase of the cycle. The snapshots show the situation when the symmetric with respect to the equator $m=1$ mode dominates at the surface. In the deep layers the general distribution of the non-axisymmetric magnetic field is close to model M1.

The stationary dynamo evolution begins about 15 years after the initialization of the non-axisymmetric magnetic field in model M1 (see Fig.5). The relaxation time of model M2 is about 20 years. In the stationary stage the non-axisymmetric field is concentrated at the top of the convection zone like in the snapshots shown in Figures 7 and 8 (also see Figures 5(a) and 6(a)). The antisymmetric $m=1$ mode dominates in both models.

To investigate the rotation rate of the non-axisymmetric modes we calculate power spectra of the $m=1$ mode azimuth for different radii. Figure 10 shows results for the three levels of the solar convection zone. The time series cover the period about 5 year after the initialization of the non-axisymmetric field in the models. At the initialization period the equatorial dipole was rotating with a period of 27.26 days, which corresponds to the differential rotation period at the latitude of the maxima of the initial perturbation. For model M1 it is found that in the subsurface shear layer the equatorial dipole rotates with the periods of 25.1-25.5 days. This corresponds to rotation of the subsurface shear layer at the 30° latitude. At the surface the dipole rotates with the period about 25.7 days, and at the bottom of the convection zone it rotates with the period of 25.1 days. The origin of these rotational periods has to be studied further. It seems that the periods of rotation follows the rotation profile in the solar convection zone, e.g., see the typical bow of the magnetic field distribution in Fig 9(c). In model M2 the meridional circulation mixes all the layers of the convection zone producing a unique maximum of the nonaxisymmetric magnetic field rotating with period of 25.4 days, which correspond to the differential rotation period at latitude of 30° and $r = 0.9R$.

4. Discussion and Summary

In the paper we explored the evolution of a non-axisymmetric magnetic field perturbations in the mean-field solar-type dynamo models. The models are kinematic with respect to the mean flow. The distribution of the mean flow is taken from the recent results of helioseismology, including the subsurface rotational shear layer and the double-cell meridional circulation pattern which was suggested recently by results of Zhao et al. (2013). We studied models with and without meridional circulation. The non-axisymmetric dynamo model takes into account the mean turbulent electromotive force in a fairly complete form. The mean electromotive force which is employed in the non-axisymmetric part of the model is the same as for the axisymmetric part except that the δ -effect ($\Omega \times J$ term) (Rädler 1969) was omitted in the non-axisymmetric electromotive force. We plan to investigate it separately.

Earlier it was found that excitation of the large-scale non-axisymmetric field on the Sun and solar-type stars is possible due to the non-linear α -effect (Raedler et al. 1990; Moss et al. 1991; Moss 1999). These models predicted a weak non-axisymmetric field for the solar case. The main reason for this is that the differential rotation on the Sun is rather strong and efficiently cascades the non-axisymmetric field to the smaller scales at which it dissipated by the turbulent diffusion dissipate it before the dynamo instability starts (Raedler et al. 1990). The non-linear α -effect couples the evolution of the axisymmetric and non-axisymmetric parts of the field. Thus, the non-axisymmetric dynamo can be maintained in expense of the energy of the axisymmetric magnetic field.

We considered non-axisymmetric dynamo models including the non-linear magnetic helicity and magnetic buoyancy effects, which were not studied before. The study confirms the previous findings of Moss (1999) that the non-axisymmetric dynamo component is rather weak if we start from a weak initial (seed) non-axisymmetric field. We notice that

our models can be characterized as weakly non-linear because the parameter of the α -effect in the model is only 30% above the dynamo instability threshold. Also the magnetic helicity conservation and magnetic buoyancy prevent the generation of magnetic field of the super-equipartition strength (Brandenburg & Käpylä 2007; Hubbard & Brandenburg 2012). Thus the low-strength non-axisymmetric magnetic field generated from a weak seed field can be explained by the linear stability of the non-axisymmetric field and the weak non-linearity of the dynamo system. However, finite-amplitude non-axisymmetric perturbations, which can be developed in the complex dynamical system may have significant effects.

The paper concentrates on illustrating the effect of a non-axisymmetric perturbation on the axisymmetric dynamo and the subsequent evolution of the non-axisymmetric magnetic field. In addition to models M1 and M2 presented in the paper, we run the models for different initial conditions by changing the spatial distribution of the non-axisymmetric perturbation and initialization time relative to the different epochs of the magnetic cycle. In model M1 the effect of perturbation is the greatest when it is initiated at the growing phase of the cycle. Also, the impact of the perturbation, and the amplitude of the non-axisymmetric field after the relaxation are stronger with the increase of the perturbation depth. However, if the perturbation in the form of Eq(24) is localized near the bottom of the convection zone, it produces only a weak effect on the large-scale distributed dynamo.

Model M2 has a long overlap between the subsequent cycle (see Fig.3). Therefore we did not investigate in details the question about impact of the initiation phase of perturbation on the dynamo. The other conclusions which we mentioned discussing effects of the initial conditions for model M1 are valid for model M2 as well.

The modeling results show that effect of the magnetic helicity conservation (dynamical quenching of the α -effect) is an important factor to preserve the non-axisymmetric field

from a complete decay. The evolution of the magnetic helicity density (Eq 16) depends on the magnetic Reynolds number, R_m , which is a free parameter of the model. We made model runs varying R_m in the range 10^4 to 10^6 . It is found that the magnitude of transient cycle is about fifty percent larger in case of $R_m = 10^4$ than in the case of $R_m = 10^6$. In this case the relaxation evolves in the same way as for $R_m = 10^4$. However in the case of $R_m = 10^6$ the magnetic cycles which establish after the transient cycle have about 20% smaller amplitude than the original cycle. This happens because the magnetic helicity, which is better conserved in case $R_m = 10^6$ than for $R_m = 10^4$, quenches of the generation magnetic field by the α -effect.

Also, our models include nonlinear effects of magnetic buoyancy. It is found that if the magnetic buoyancy is switched off then the strength of the non-axisymmetric field after the relaxation is by factor two smaller.

It is interesting that the models without meridional circulation show the non-axisymmetric field distribution in a form of persistent “active longitudes” when the relaxation phase of evolution is passed. The models show that the non-axisymmetric field undergoes “flip-flops” around these longitudes during the decaying phase of the magnetic cycle. The origin of these longitudes and flip-flop phenomena in nonlinear non-axisymmetric dynamo was discussed in details by Moss (2004) (see, also, discussion in Berdyugina et al. 2006). In our calculations the active longitude is fixed when the $T_{1,1}$ and $S_{1,1}$ dynamo-modes are in phase or in anti-phase. The flip-flop occurs when the orientation of the equatorial dipole changes the sign. If this effect is accompanied by the equatorial symmetry variations of the axisymmetric magnetic field then the orientation of the large-scale magnetic field changes by 180° .

Rotation of the non-axisymmetric magnetic field harmonics is rather important for the purpose of dynamo diagnostics. Bigazzi & Ruzmaikin (2004) found the periods of 26.18

days in their linear non-axisymmetric model with the α -effect distributed in the convection zone. They found a period of 26.7 days for the model with the α -effect concentrated at the top of the convection zone. Our model without meridional circulation shows different rotational periods of the $T_{1,1}$ and $S_{1,1}$ modes for the different levels of the solar convection zone. The $T_{1,1}$ mode at $r = 0.9R_{\odot}$ has the rotational periods ranging from 25.1 to 25.5 days. At the bottom of the convection zone it rotates with the period of about 25.1 days. At the surface these modes rotate slower, with the period of 25.7 days. The meridional circulation mixes the dynamo modes through all layers of the convection zone producing a common rotational period of 25.4 days, which correspond to latitude of about 30° at $r = 0.9R_{\odot}$. After the relaxation is passed the active longitude rotates with the sidereal period of 27.2 days.

The paper illustrates initial results of the nonlinear non-axisymmetric mean-field dynamo model. The axisymmetric part of the model is based on our previous results. For the first time we demonstrate that nonlinear coupling between the asymmetric and the non-axisymmetric field can impact the generation of the axisymmetric field in the case of finite-amplitude perturbations. The effect depends strongly on the dynamo mechanisms involved in the problem, the spatial distribution of perturbation, conditions of the dynamo processes at the time and how well the magnetic helicity is conserved in the system. These factors determine the subsequent evolution of the dynamo system including the cycle of the axisymmetric dynamo, evolution and rotation of the non-axisymmetric modes of large-scale magnetic fields.

In summary:

- In the solar dynamo models non-axisymmetrical perturbations decay and can be maintained only at low amplitude because of nonlinear turbulent effects.
- Without meridional circulation the non-axisymmetric dynamo-mode can show the

active longitude “flip-flop” phenomenon. The solar-type (double-cell) meridional circulation destroys this effect.

- Periods of rotation of the non-axisymmetric modes depend on the the internal differential rotation and distribution of the magnetic field strength, and provide important information about dynamo process.

Acknowledgements The work was partially supported by NASA grants NNX09AJ85G and NNX14AB70G. VP thanks support of RFBR under grants 14-02-90424, 15-02-01407 and the project II.16.3.1 of ISTP SB RAS.

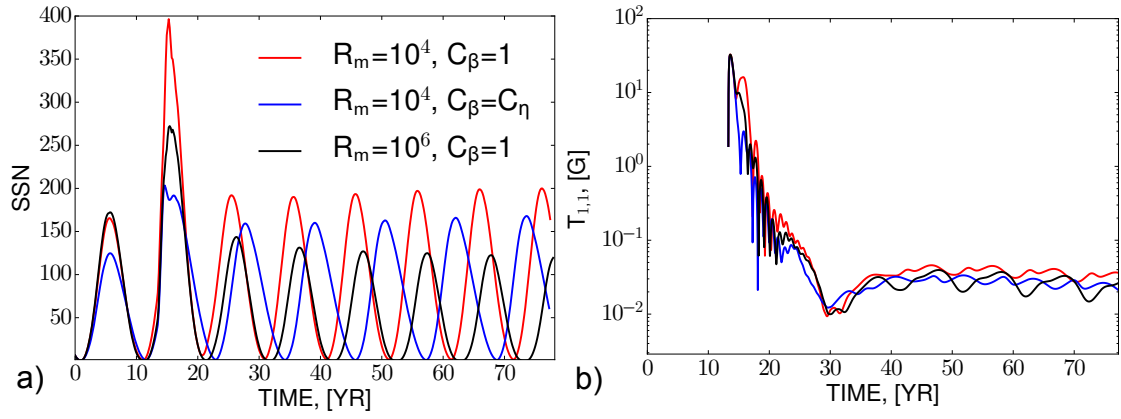


Fig. 4.— Evolution of the simulated sunspot number (a) and $T_{1,1}$ harmonic (b) in model M1 for the different values of the parameter R_m and C_β : $R_m = 10^4$, $C_\beta = 1$ (red), $R_m = 10^4$, $C_\beta = C_\eta$ (blue), $R_m = 10^6$, $C_\beta = 1$ (black).

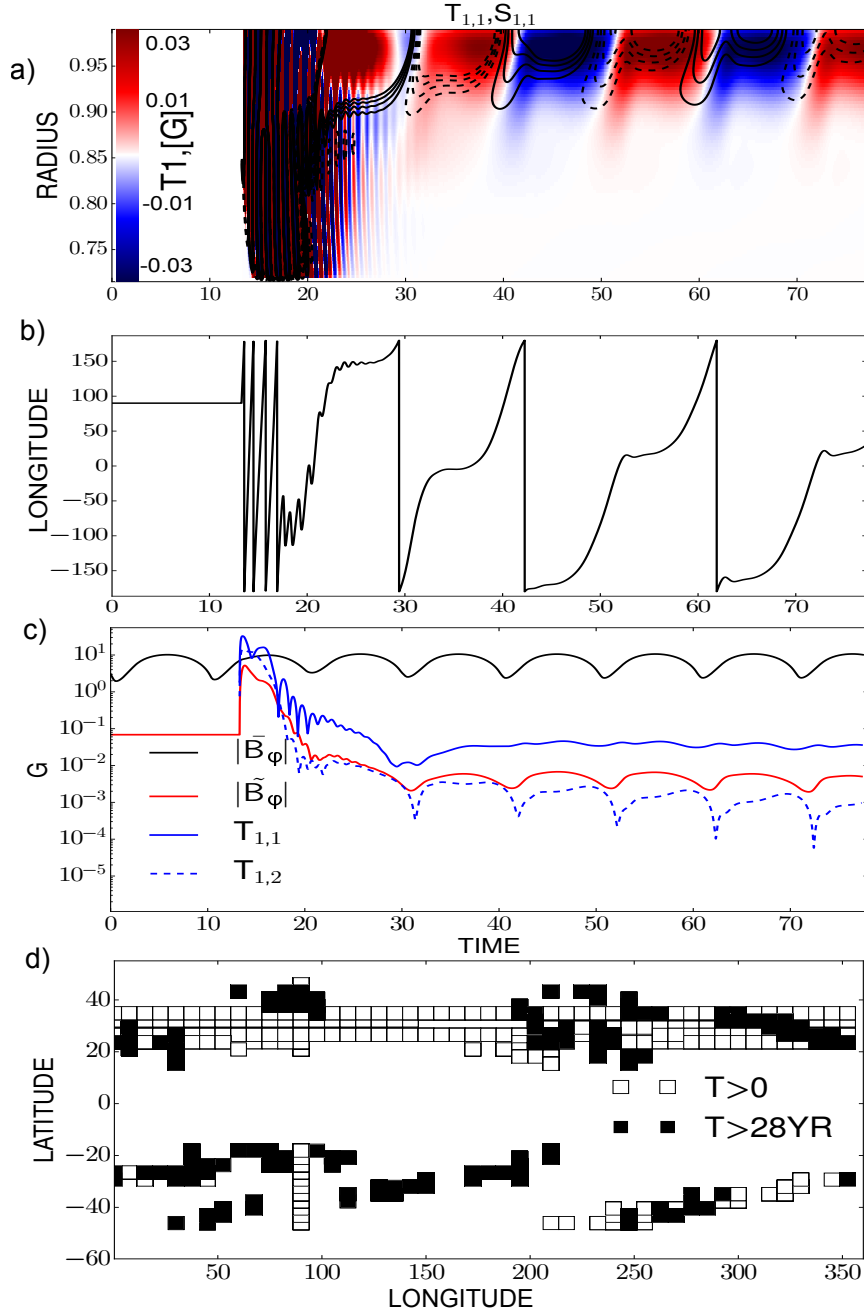


Fig. 5.— Non-axisymmetric modes of model M1: a) the time-radius evolution of the dynamo modes $T_{1,1}$ (background image) and $S_{1,1}$ modes (contours are in the same range of values as the color scale); b) evolution of longitude of the maximum of the large-scale toroidal field, c) the mean strength of the near-surface axisymmetric and non-axisymmetric toroidal magnetic field and the strength of the $m=1$ T-potentials, d) position of maxima of the total toroidal magnetic field strength of the subsurface shear layer ($r=0.92R$). Filled squares correspond to the relaxed state ($t > 28$ yr), 15 years after the initialization of the non-axisymmetric perturbation

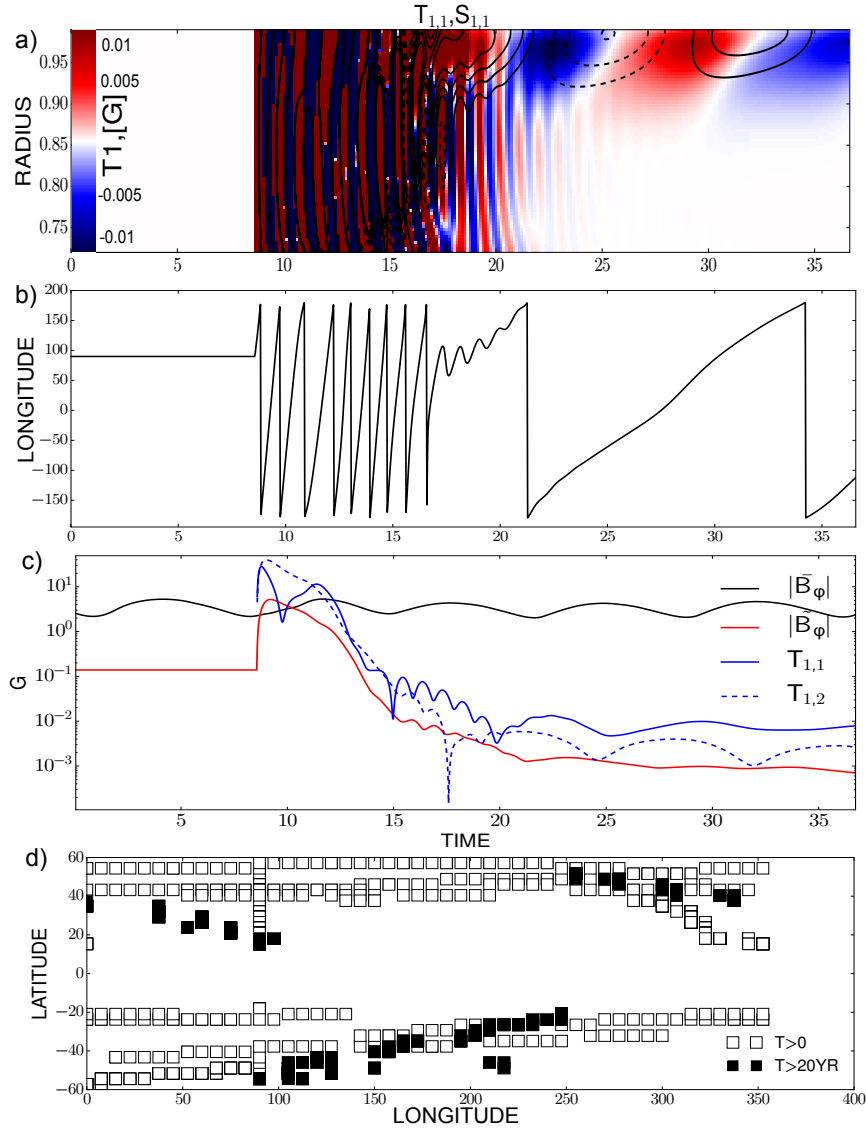


Fig. 6.— The same as Figure 5 for model M2

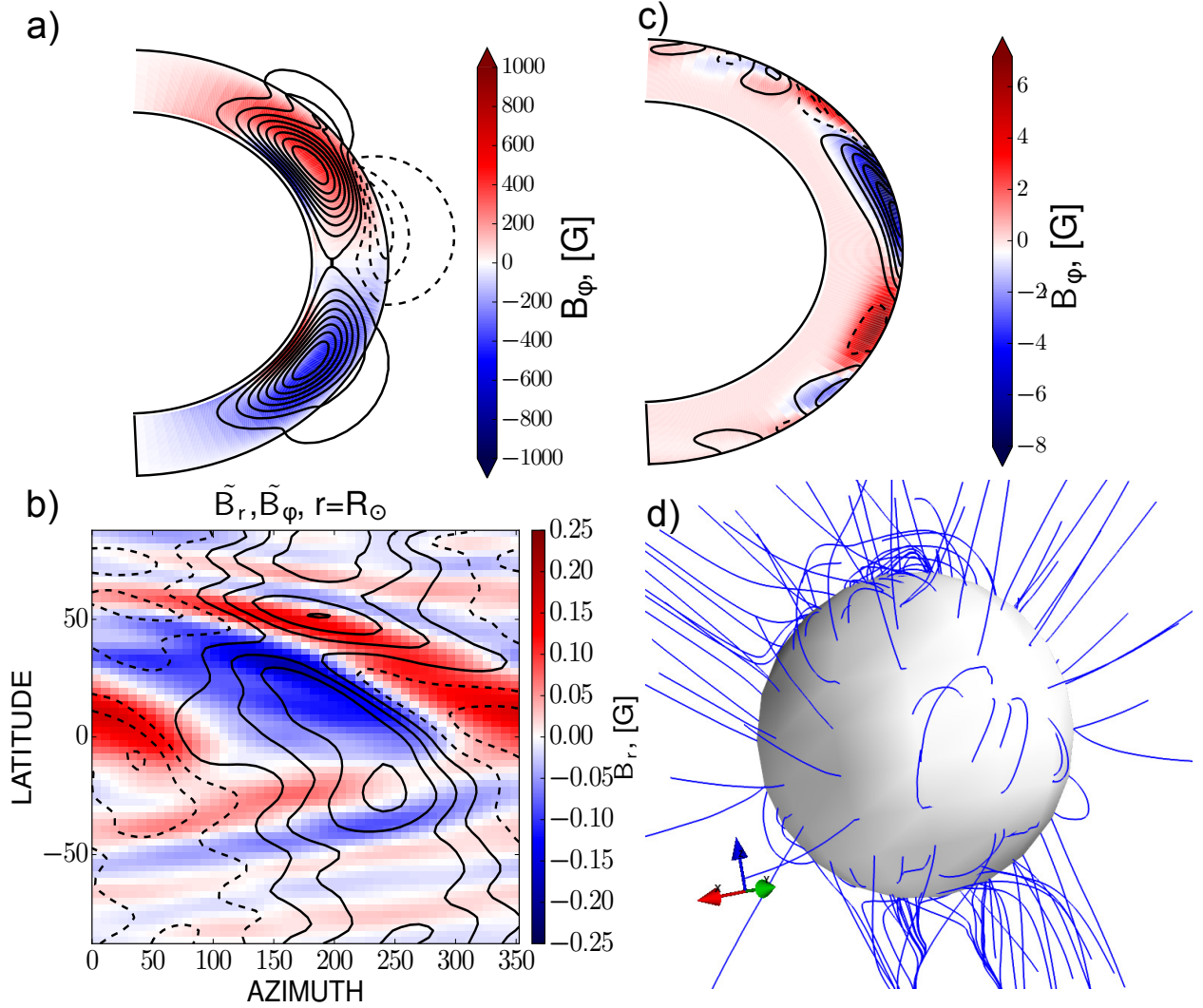


Fig. 7.— Model M1 half year after the initialization of the non-axisymmetric perturbation, a) distribution of the axisymmetric toroidal magnetic field (background image) and poloidal field lines in the meridional cross-section, b) azimuth-latitude distribution of the non-axisymmetric radial magnetic field (background image) and toroidal magnetic field (contours are in the same range as the colorscale) on the surface; c) the same as in panel (a) for the non-axisymmetric components of magnetic field; d) the magnetic field lines of the non-axisymmetric magnetic field above the surface.

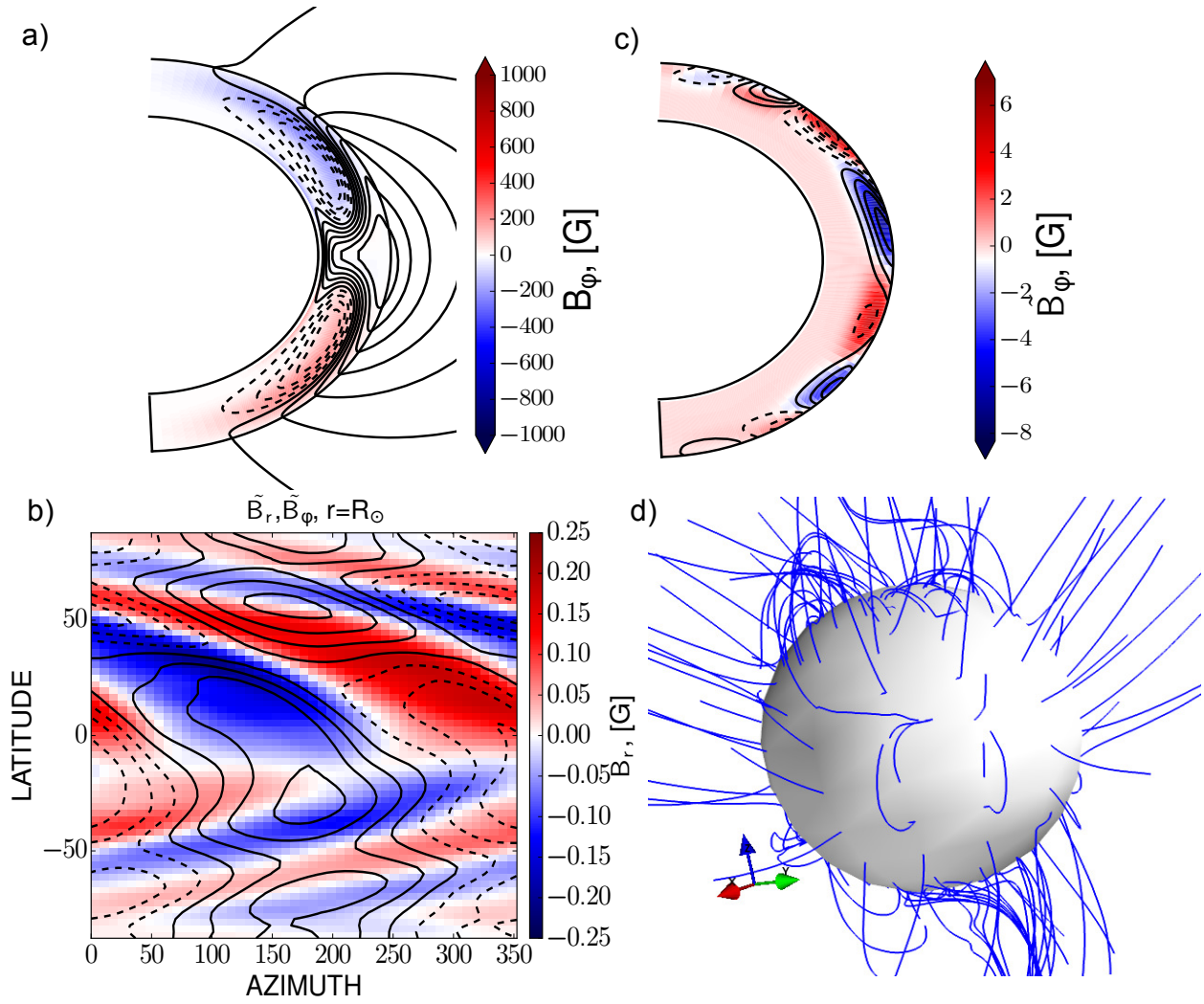


Fig. 8.— The same as Figure 7 for model M2

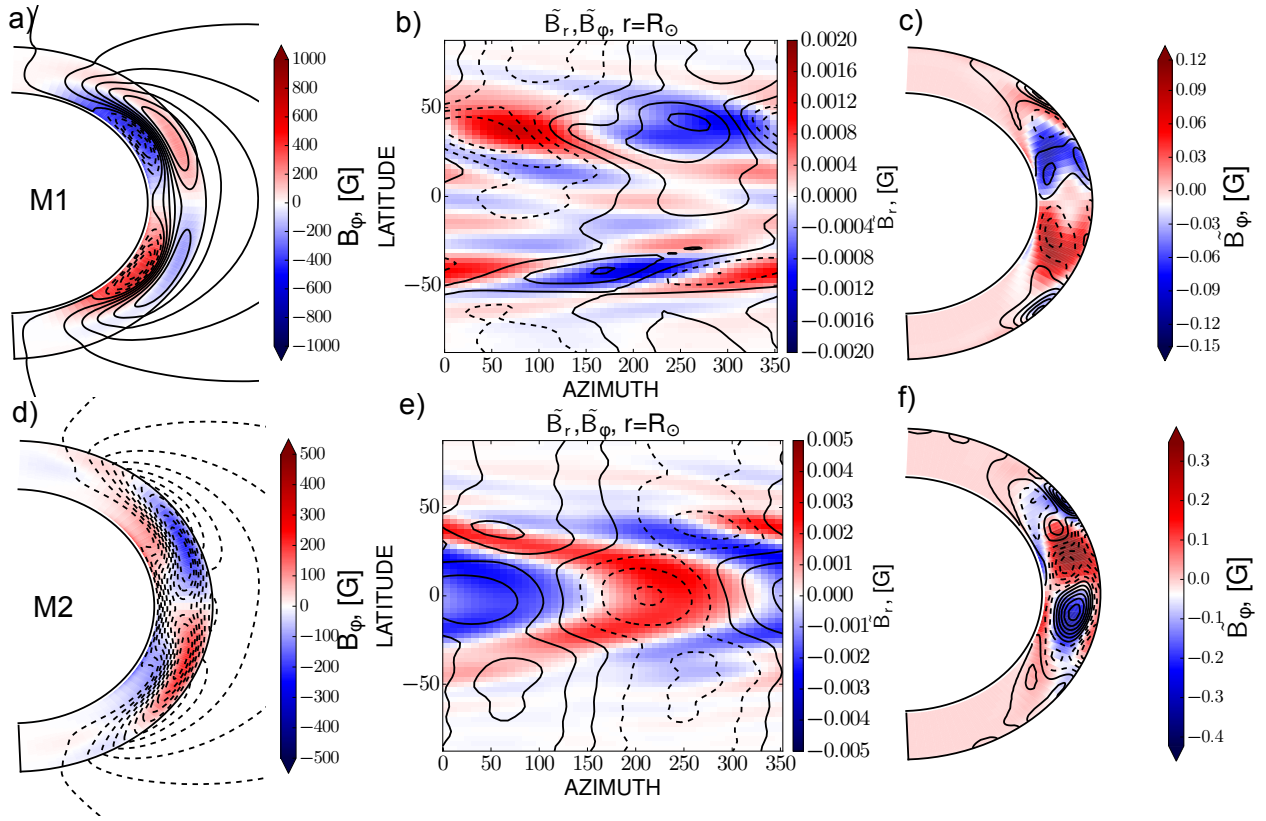


Fig. 9.— The same as in Fig. 7 after 5 years of the evolution after the initialization of the non-axisymmetric perturbation.

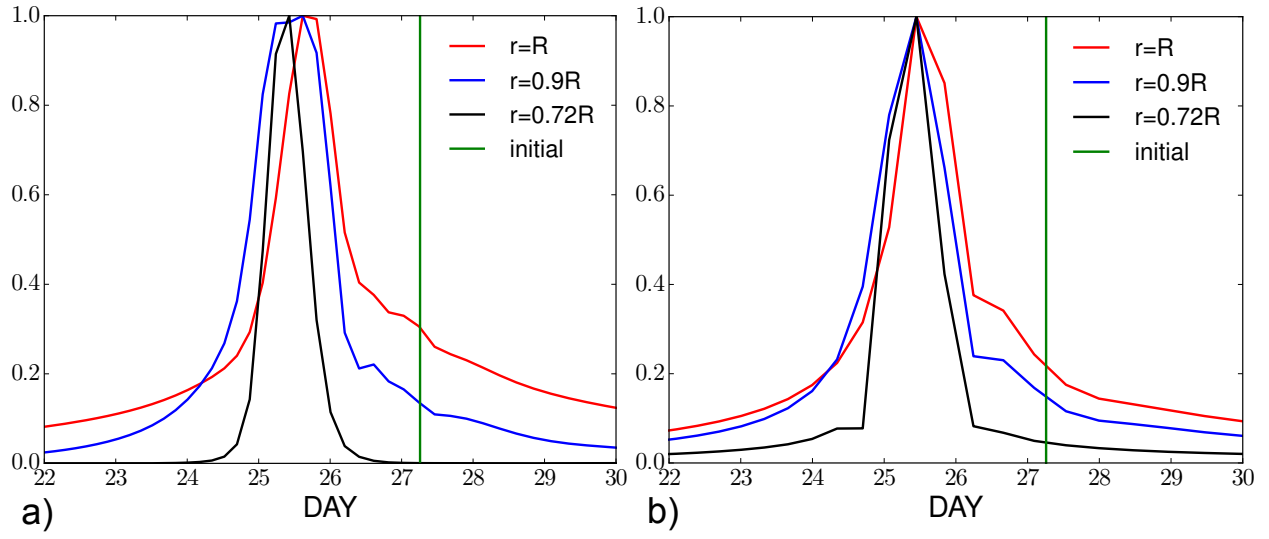


Fig. 10.— The normalized power spectra for rotation periods of azimuth of non-axisymmetric mode $S_{1,1}$ at the three levels in the solar convection zone for: a) model M1; b) model M2.

REFERENCES

- Abramenko, V. I., Carbone, V., Yurchyshyn, V., Goode, P. R., Stein, R. F., Lepreti, F., Capparelli, V., & Vecchio, A. 2011, *ApJ*, 743, 133
- Antonucci, E., Hoeksema, J. T., & Scherrer, P. H. 1990, *ApJ*, 360, 296
- Berdyugina, S. V. 2004, *Sol. Phys.*, 224, 123
- Berdyugina, S. V., Moss, D., Sokoloff, D., & Usoskin, I. G. 2006, *A&A*, 445, 703
- Bigazzi, A., & Ruzmaikin, A. 2004, *ApJ*, 604, 944
- Blackman, E. G., & Field, G. B. 2002, *Phys. Rev. Lett.*, 89
- Brandenburg, A., & Käpylä, P. J. 2007, *New Journal of Physics*, 9, 305
- Brandenburg, A., & Subramanian, K. 2005, *Phys. Rep.*, 417, 1
- Dikpati, M., & Gilman, P. A. 2001, *ApJ*, 559, 428
- Duvall, Jr., T. L., Scherrer, P. H., Svalgaard, L., & Wilcox, J. M. 1979, *Sol. Phys.*, 61, 233
- Elstner, D., & Korhonen, H. 2005, *Astronomische Nachrichten*, 326, 278
- Frisch, U., Pouquet, A., Léorat, J., & A., M. 1975, *J. Fluid Mech.*, 68, 769
- Gyenge, N., Baranyi, T., & Ludmány, A. 2012, *Central European Astrophysical Bulletin*, 36, 9
- Hoeksema, J. T. 1995, *Space Sci. Rev.*, 72, 137
- Howe, R., Larson, T. P., Schou, J., Hill, F., Komm, R., Christensen-Dalsgaard, J., & Thompson, M. J. 2011, *Journal of Physics Conference Series*, 271, 012061
- Hubbard, A., & Brandenburg, A. 2012, *ApJ*, 748, 51

- Kichatinov, L. L. 1991, *Astron. Astrophys.*, 243, 483
- Kichatinov, L. L., & Pipin, V. V. 1993, *A&A*, 274, 647
- Kleorin, N., & Rogachevskii, I. 2003, *Phys. Rev. E*, 67, 026321
- Kleorin, N. I., & Ruzmaikin, A. A. 1982, *Magnetohydrodynamics*, 18, 116
- Krause, F., & Rädler, K.-H. 1980, *Mean-Field Magnetohydrodynamics and Dynamo Theory* (Berlin: Akademie-Verlag), 271
- Krivodubskij, V. N. 1987, *Soviet Astronomy Letters*, 13, 338
- Kuzanyan, K. M., Pipin, V. V., & Seehafer, N. 2006, *Sol.Phys.*, 233, 185
- Mitra, D., Candelaresi, S., Chatterjee, P., Tavakol, R., & Brandenburg, A. 2010, *Astronomische Nachrichten*, 331, 130
- Moffatt, H. K. 1978, *Magnetic Field Generation in Electrically Conducting Fluids* (Cambridge, England: Cambridge University Press)
- Moss, D. 1999, *MNRAS*, 306, 300
- . 2004, *MNRAS*, 352, L17
- Moss, D., Tuominen, I., & Brandenburg, A. 1991, *A&A*, 245, 129
- Muciaccia, P. F., Natoli, P., & Vittorio, N. 1997, *ApJ*, 488, L63
- Parker, E. N. 1979, *Cosmical magnetic fields: Their origin and their activity* (Oxford: Clarendon Press)
- Pipin, V. V. 2008, *Geophysical and Astrophysical Fluid Dynamics*, 102, 21
- Pipin, V. V., & Kosovichev, A. G. 2011, *ApJL*, 727, L45

- Pipin, V. V., & Kosovichev, A. G. 2013, *The Astrophysical Journal*, 776, 36
- Pipin, V. V., & Kosovichev, A. G. 2014, *ApJ*, 785, 49
- Pipin, V. V., Sokoloff, D. D., & Usoskin, I. G. 2012, *A&A*, 542, A26
- Pipin, V. V., Zhang, H., Sokoloff, D. D., Kuzanyan, K. M., & Gao, Y. 2013, *MNRAS*, 435, 2581
- Pouquet, A., Frisch, U., & Léorat, J. 1975, *J. Fluid Mech.*, 68, 769
- Rädler, K.-H. 1969, *Monats. Dt. Akad. Wiss.*, 11, 194
- Rädler, K.-H., Kleorin, N., & Rogachevskii, I. 2003, *Geophys. Astrophys. Fluid Dyn.*, 97, 249
- Raedler, K.-H. 1986, *Astronomische Nachrichten*, 307, 89
- Raedler, K.-H., Wiedemann, E., Brandenburg, A., Meinel, R., & Tuominen, I. 1990, *A&A*, 239, 413
- Rogachevskii, I., Kleorin, N., Käpylä, P. J., & Brandenburg, A. 2011, *Phys. Rev. E*, 84, 056314
- Stix, M. 2002, *The sun: an introduction*, 2nd edn. (Berlin : Springer), 521
- Tuominen, I., Berdyugina, S. V., & Korpi, M. J. 2002, *Astronomische Nachrichten*, 323, 367
- Twoiewski, A., Covas, E., Tavakol, R., & Brandenburg, A. 1998, *ArXiv Astrophysics e-prints*
- Zhao, J., Bogart, R. S., Kosovichev, A. G., Duvall, Jr., T. L., & Hartlep, T. 2013, *ApJ*, 774, L29

5. Appendix A

5.1. Mean-ectromotive force \mathcal{E}

This section of Appendix describe some parts of the mean-electromotive force. We employ the anisotropic diffusion tensor which is derived by Pipin (2008) (hereafter P08) and Pipin & Kosovichev (2014):

$$\begin{aligned} \eta_{ijk} = & 3\eta_T \left\{ \left(2f_1^{(a)} - f_2^{(d)} \right) \varepsilon_{ijk} + 2f_1^{(a)} e_i e_n \varepsilon_{jnk} \right. \\ & \left. + \frac{a}{3} \phi_1 (g_n g_j \varepsilon_{ink} - \varepsilon_{ijk}) \right\} + 3\eta_T C_\delta f_4^{(d)} e_j \left\{ \tilde{\varphi}_7^{(w)} \delta_{ik} + \tilde{\varphi}_2^{(w)} \frac{\overline{B_i B_k}}{\overline{B^2}} \right\}, \end{aligned} \quad (\text{A1})$$

where $\mathbf{e} = \mathbf{\Omega}/\Omega$ is the unit vector along the rotation axis, and \mathbf{g} is the unit vector in the radial direction, a is the parameter of the turbulence anisotropy, η_T is the magnetic diffusion coefficient. The diffusivity coefficients depend on the Coriolis number $\Omega^* = 4\pi \frac{\tau_c}{P_{rot}}$, where P_{rot} is the rotational period, τ_c is the convective turnover time. The quenching functions $f_{1,2}^{(a,d)}$ and ϕ_1 are

$$\begin{aligned} f_1^{(a)} &= \frac{1}{4\Omega^{*2}} \left((\Omega^{*2} + 3) \frac{\arctan \Omega^*}{\Omega^*} - 3 \right), \\ f_2^{(d)} &= \frac{1}{\Omega^{*2}} \left(\frac{\arctan \Omega^*}{\Omega^*} - 1 \right), \\ \phi_1 &= -\frac{1}{24\Omega^{*2}} (2 \log(1 + 4\Omega^{*2}) + 4 \log(1 + \Omega^{*2}) \\ &\quad + (1 - 4\Omega^{*2}) \frac{\arctan(2\Omega^*)}{\Omega^*} + 4(1 - \Omega^{*2}) \frac{\arctan(\Omega^*)}{\Omega^*} - 6). \end{aligned}$$

The last term in Eq.(A1) is a contribution of the $\mathbf{\Omega} \times \mathbf{J}$ effect with a free parameter C_δ and the quenching functions of the magnetic field and the Coriolis number, $\tilde{\varphi}_{2,7}^{(w)}(\beta)$ and

$f_4^{(d)}(\Omega^*)$:

$$\tilde{\varphi}_2^{(w)} = -\frac{5}{192\beta^5} \left(3(16\beta^4 - 5) \frac{\arctan(2\beta)}{2\beta} - 5(4\beta^2 - 3) \right), \quad (\text{A2})$$

$$\tilde{\varphi}_7^{(w)} = \frac{5}{192\beta^4} \left(3(16\beta^4 - 1) \frac{\arctan(2\beta)}{2\beta} - (4\beta^2 - 3) \right), \quad (\text{A3})$$

$$f_4^{(d)} = \frac{1}{6\Omega^{*3}} \left((2\Omega^{*2} + 3) - 3(\Omega^{*2} + 1) \frac{\arctan(\Omega^*)}{\Omega^*} \right). \quad (\text{A4})$$

Note that in the notation of P08 $\tilde{\varphi}_{2,7}^{(w)}(\beta) = \frac{5}{2}\varphi_{2,7}^{(w)}(\beta)$ and $\beta = \frac{|\overline{B}|}{\sqrt{4\pi\bar{\rho}u^2}}$.

The α effect takes into account the kinetic and magnetic helicities,

$$\alpha_{ij} = C_\alpha \sin^2 \theta \psi_\alpha(\beta) \alpha_{ij}^{(H)} \eta_T + \alpha_{ij}^{(M)} \frac{\bar{\chi} \tau_c}{4\pi \bar{\rho} \ell^2} \quad (\text{A5})$$

where C_α is a free parameter, the $\alpha_{ij}^{(H)}$ and $\alpha_{ij}^{(M)}$ express the kinetic and magnetic helicity parts of the α -effect, respectively, $\bar{\chi}$ is the small-scale magnetic helicity and ℓ is the typical length scale of the turbulence. The $\alpha_{ij}^{(H)}$ reads,

$$\begin{aligned} \alpha_{ij}^{(H)} &= \delta_{ij} \left\{ 3 \left(f_{10}^{(a)} (\mathbf{e} \cdot \mathbf{\Lambda}^{(\rho)}) + f_{11}^{(a)} (\mathbf{e} \cdot \mathbf{\Lambda}^{(u)}) \right) \right\} + \\ &+ e_i e_j \left\{ 3 \left(f_5^{(a)} (\mathbf{e} \cdot \mathbf{\Lambda}^{(\rho)}) + f_4^{(a)} (\mathbf{e} \cdot \mathbf{\Lambda}^{(u)}) \right) \right\} \\ &+ 3 \left\{ \left(e_i \Lambda_j^{(\rho)} + e_j \Lambda_i^{(\rho)} \right) f_6^{(a)} + \left(e_i \Lambda_j^{(u)} + e_j \Lambda_i^{(u)} \right) f_8^{(a)} \right\}. \end{aligned} \quad (\text{A6})$$

and the $\alpha_{ij}^{(M)}$ reads:

$$\alpha_{ij}^{(M)} = 2f_2^{(a)} \delta_{ij} - 2f_1^{(a)} e_i e_j, \quad (\text{A7})$$

Below we give the functions of the Coriolis number defining the dependence of the α -effect

on the Coriolis number:

$$f_2^{(a)} = \frac{1}{4\Omega^{*2}} \left((\Omega^{*2} + 1) \frac{\arctan \Omega^*}{\Omega^*} - 1 \right), \quad (\text{A8})$$

$$f_3^{(a)} = \frac{1}{4\Omega^{*2}} \left(2 - 2 \frac{\arctan \Omega^*}{\Omega^*} \right), \quad (\text{A9})$$

$$f_4^{(a)} = \frac{1}{6\Omega^{*3}} \left(3 (\Omega^{*4} + 6\Omega^{*2} + 5) \frac{\arctan \Omega^*}{\Omega^*} - (13\Omega^{*2} + 15) \right), \quad (\text{A10})$$

$$f_5^{(a)} = \frac{1}{\Omega^*} \left((\Omega^{*2} + 3) \frac{\arctan \Omega^*}{\Omega^*} - 3 \right), \quad (\text{A11})$$

$$f_6^{(a)} = \frac{1}{6\Omega^{*3}} \left(3 (\Omega^{*2} + 2) \frac{\arctan \Omega^*}{\Omega^*} - (\Omega^{*2} + 6) \right), \quad (\text{A12})$$

$$f_8^{(a)} = -\frac{1}{12\Omega^{*3}} \left(3 (4\Omega^{*2} + 2) \frac{\arctan \Omega^*}{\Omega^*} - (10\Omega^{*2} + 6) \right), \quad (\text{A13})$$

$$f_{10}^{(a)} = \frac{1}{\Omega^*} \left(1 - (\Omega^{*2} + 1) \frac{\arctan \Omega^*}{\Omega^*} \right), \quad (\text{A14})$$

$$f_{11}^{(a)} = -\frac{1}{6\Omega^{*3}} \left(3 (\Omega^{*2} + 1)^2 \frac{\arctan \Omega^*}{\Omega^*} - (5\Omega^{*2} + 3) \right), \quad (\text{A15})$$

The functions (A8-A15) were defined in P08 for the general case which includes the effects the hydrodynamic and magnetic fluctuations in the background turbulence. Here, we bring the expressions for the case when the background turbulent fluctuations of the small-scale magnetic field are in the equipartition with the hydrodynamic fluctuations, i.e., $\varepsilon = \frac{b'^2}{4\pi\bar{\rho}u'^2} = 1$, where the u'^2 and b'^2 are intensity of the background turbulent velocity and magnetic field. The magnetic quenching function of the hydrodynamical part of α -effect is defined by

$$\psi_\alpha = \frac{5}{128\beta^4} \left(16\beta^2 - 3 - 3(4\beta^2 - 1) \frac{\arctan(2\beta)}{2\beta} \right). \quad (\text{A16})$$

Note in the notation of P08 $\psi_\alpha = -3/4\phi_6^{(a)}$.

The turbulent pumping of the mean-field contains the sum of the contributions due to the mean density gradient (Kichatinov 1991), $\gamma_{ij}^{(\rho)}$, the diamagnetic pumping (Krivodubskij 1987), $\gamma_{ij}^{(\eta)}$, the mean-field magnetic buoyancy (Kichatinov & Pipin 1993), $\gamma_{ij}^{(b)}$, and due to

effects of the large-scale shear (Rogachevskii et al. 2011), $\gamma_{ij}^{(H)}$:

$$\gamma_{ij} = \gamma_{ij}^{(\rho)} + \gamma_{ij}^{(\eta)} + \gamma_{ij}^{(b)} + \gamma_{ij}^{(H)}, \quad (\text{A17})$$

where each contribution is defined as follows:

$$\gamma_{ij}^{(\rho)} = 3\eta_T \left\{ f_3^{(a)} \Lambda_n^{(\rho)} + f_1^{(a)} \left(\mathbf{e} \cdot \mathbf{\Lambda}^{(\rho)} \right) e_n \right\} \varepsilon_{inj} \quad (\text{A18})$$

$$-3\eta_T f_1^{(a)} e_j \varepsilon_{inm} e_n \Lambda_m^{(\rho)}$$

$$\gamma_{ij}^{(\eta)} = \frac{3}{2} \eta_T \left\{ f_2^{(a)} \Lambda_n^{(\eta)} \varepsilon_{inj} + f_1^{(a)} e_j \varepsilon_{inm} e_n \Lambda_m^{(\eta)} \varepsilon_{inm} \right\} \quad (\text{A19})$$

$$\gamma_{ij}^{(b)} = \frac{\alpha_{MLT} u'}{\gamma} \beta^2 K(\beta) g_n \varepsilon_{inj}, \quad (\text{A20})$$

$$\gamma_{ij}^{(H)} = \left(f_2^{(\gamma)} \frac{\bar{\chi}}{\rho \ell^2} + f_1^{(\gamma)} h_{\mathcal{K}} \right) \tau_c^2 \varepsilon_{ikj} \bar{W}_k \quad (\text{A21})$$

where $f_{1,2,3}^{(a)}(\Omega^*)$ and $f_{1,2}^{(\gamma)}(\Omega^*)$ - are functions of the Coriolis number, u' is the RMS of the convective velocity, $\Lambda_i^{(\rho)} = \nabla_i \log \bar{\rho}$ are components of the gradient of the mean density, $\Lambda_i^{(\eta)} = \nabla_i \log \eta_T$ is the same for the turbulent diffusivity. The α_{MLT} is the parameter of the mixing length theory, γ is the adiabatic exponent, C_β is a free parameter to switch on/off the effect in the model and \mathbf{g} is the unit vector in the radial direction. The quenching of the magnetic buoyancy (see (Kichatinov & Pipin 1993)) is determined by

$$K = \frac{1}{16\beta^4} \left(\frac{(\beta^2 - 3)}{\beta} \arctan(\beta) + \frac{(\beta^2 + 3)}{(\beta^2 + 1)} \right).$$

The pumping effect $\gamma_{ij}^{(H)}$ is determined by the helicity parameters including the magnetic, $\bar{\chi}$, and kinetic helicity, $h_{\mathcal{K}} = \frac{3\eta_T}{2\tau_c} F_1(\Omega^*) \cos \theta \frac{\partial}{\partial r} \log(\bar{\rho} u')$ (see, Kuzanyan et al. 2006), and the large-scale vorticity vector $\bar{\mathbf{W}} = \nabla \times \bar{\mathbf{U}}$. Dependence of the $\gamma_{ij}^{(H)}$ on the Coriolis number is controlled by the quenching functions:

$$f_1^{(\gamma)} = \frac{1}{(24\Omega^*)^2} \left((1300\Omega^{*2} + 391) \frac{\arctan(2\Omega^*)}{2\Omega^*} - 1456(\Omega^{*2} + 1) \frac{\arctan(\Omega^*)}{\Omega^*} - 3(32\Omega^{*2} - 355) \right), \quad (\text{A22})$$

$$F_1 = \frac{1}{2\Omega^*} \left((\Omega^{*2} - 1) \frac{\arctan \Omega^*}{\Omega^*} + 1 \right) \quad (\text{A23})$$

and $f_2^{(\gamma)} = 3f_2^{(a)}$.